Title	Evaluation of cross-beam vector Doppler ultrasound systems for accurate 3-D velocity measurements
Author(s)	Hussain, B; Wong, EY; Yiu, BYS; Yu, ACH; Poepping, TL
Citation	The 2012 IEEE International Ultrasonics Symposium (IUS 2012), Dresden, Germany, 7-10 October 2012. In IEEE Ultrasonics Symposium Proceedings, 2012, p. 326-329
Issued Date	2012
URL	http://hdl.handle.net/10722/189828
Rights	IEEE Ultrasonics Symposium. Proceedings. Copyright © IEEE.

10.1109/ULTSYM.2012.0080

Evaluation of Cross-beam Vector Doppler Ultrasound Systems for Accurate 3-D Velocity Measurements

B. Hussain[1], E.Y. Wong[2], B.Y.S. Yiu[3], A.C.H. Yu[3], T.L. Poepping[1,2]
Departments of Physics & Astronomy[1] and Medical Biophysics[2], University of Western Ontario, London, ON Canada
Medical Engineering Program[3], University of Hong Kong, Hong Kong
bhussai4@uwo.ca

***Abstract*—Vector Doppler ultrasound (VDUS) systems offer the potential for improved accuracy in mapping of complex flow parameters, such as recirculation, turbulence, and shear stress which are probable risk factors leading to vascular disease and stroke. Cross-beam VDUS systems were evaluated for velocity accuracy to optimize the number of receivers for the inter-beam angle, wall filter, system orientation, and complexity of flow seen in a stenosed carotid artery. Preliminary results for velocity estimation show promise for validation of numerical results.**

Keywords - vector Doppler ultrasound; carotid artery; hemodynamics; blood velocity.

I. INTRODUCTION

Doppler ultrasound (DUS) commonly is implemented as the first-line diagnostic tool to assess stroke risk from the degree of stenosis in the internal carotid artery (ICA) by measuring the jet velocities [1]. Research has shown that stenosis severity is not the sole factor for assessing stroke risk, and flow parameters, such as recirculation, turbulence, and shear stress, are also known to be potential risk factors contributing to stroke. Therefore, an accurate flow characterization is required for the prediction of stroke risk. Simultaneous 3D velocity measurements are required for accurate characterization of such parameters. Spectral DUS is limited by its 1-D nature and therefore requires the knowledge of Doppler angle. This introduces inaccurate velocity estimations, especially in regions of greater flow complexity. Vector DUS (VDUS) eliminates the need for a priori knowledge of the Doppler angle by acquiring velocity information from additional directions in 3D. VDUS with its potential to make multiple measurements in 3D is a potential tool for accurate estimation of flow parameters such as recirculation, turbulence, and shear stress.

VDUS technique was developed almost four decades ago but has not been adopted clinically. Now with the development of 2D arrays and ultrasound systems, such as Ultrasonix Sonix RP, Supersonic Imagine Aixplorer, and Verasonics, real-time 3D velocity measurements look promising. The cross-beam technique being simple in nature has its limitations of angle misregistration as well as compounding errors due to the increasing number of receivers [2, 3].

The objective of this study was to evaluate the potential of various multi-receiver configurations for accurate estimation of velocities in complex flow. Potential configurations were assessed for a range of velocity directions in 3D space by counting the number of receivers lying above the wall filter for a single low velocity magnitude. Accuracy of these configurations was assessed in a complex velocity field generated in a 50% stenosed carotid artery bifurcation. Initial experiments were performed for validation for near single peak velocity using parabolic flow generated in a large inner-diameter straight lumen.

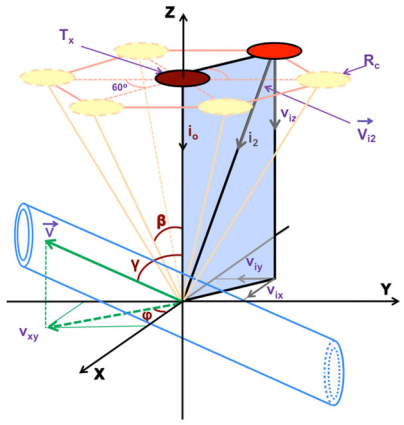

Fig. 1. An example of a VDUS system with a single central transmitter, Tx, surrounded by six receivers, Ri, with uniform spacing. V is the velocity vector, oriented at an elevation angle, γ, and an azimuth angle, φ. The inter-beam angle, β, is the angle between the transmit and a receive beam. i_o and i_2 are the unit vectors along the beams for the transmitter and a receiver,

II. METHODS

A. Numerical Evaluation of Single Velocity Estimation

A velocity of 5 cm/s was estimated based on the Doppler shifts seen by 3, 4, 5, and 6- receiver (3R, 4R, 5R, 6R) configurations using a transmit frequency of 5 MHz, 1540 m/s as the speed of sound in tissue, and a wall filter value of 50 Hz. The accuracy of velocity estimation was determined by the number of receivers with Doppler shifts above the wall filter threshold, the most accurate estimation is when three or more receivers are above the wall filter. The number of receivers were then determined for a range of velocity orientations in 3D for each of the 3R, 4R, and 6R configurations by varying inter-beam angle from 0^o to 90^o. The whole range of velocity orientation is represented by the angle the velocity vector makes with the probe axis (elevation angle, γ), ranging from 0^o to 180^o, and the angle the projection of the velocity vector makes on the xy-plane with x-axis (azimuth angle, φ), ranging from 0^o to 360^o (Fig.1).

B. Numerical Evaluation of Complex Velocity Fields

Pulsatile 3D velocity field was generated, in an idealized 50% eccentric stenosed (by NASCET criteria) [4] carotid artery

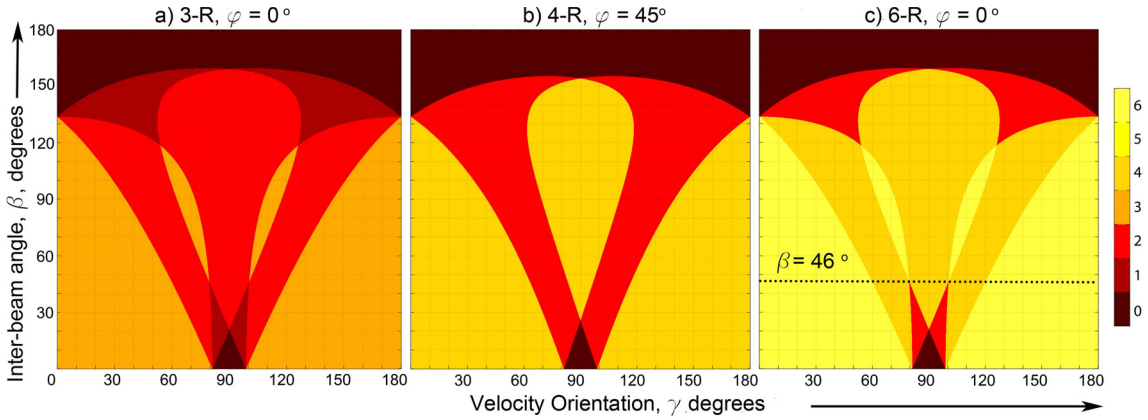

Fig. 2. Color plot representing the number of receivers with Doppler shifts above the wall filter threshold as a function of inter-beam angle, β, and velocity orientations, γ and φ, for the (a) 3-receiver, 3R, (b) 4-receiver, 4R, and (c) 6-receiver, 6R configuration

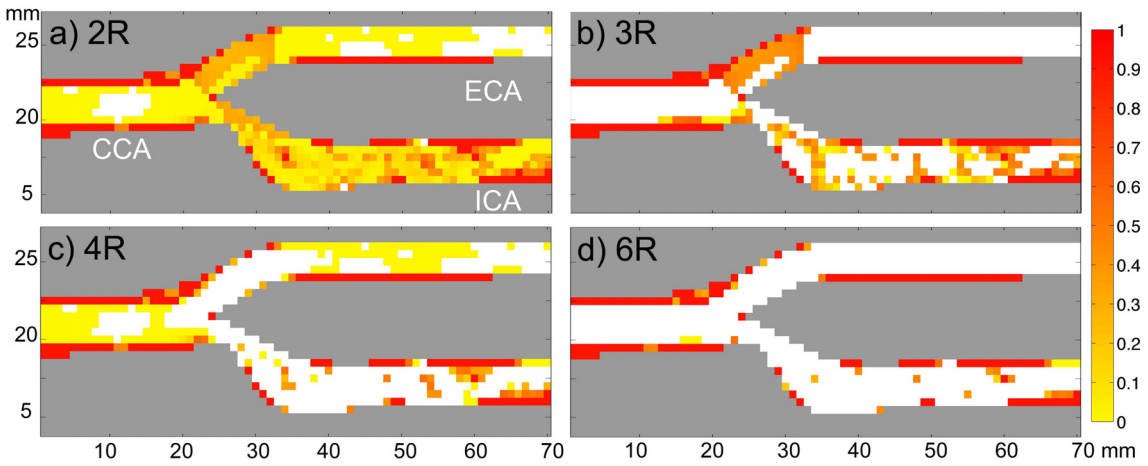

Fig. 3. Relative error in the reconstructed velocity magnitudes calculated with respect to the CFD generated velocities (reference velocity field). The errors are shown for (a) 2R, (b) 3R, (c) 4R, and (d) 6R configuration.

model, using Computational Fluid Dynamics (CFD). CFD simulations were performed using a well-validated in-house finite element solver [5, 6], with a spatial discretization of over 480,000 quadratic tetrahedral finite elements and a temporal discretization of 9600 time steps per cardiac cycle. A physiologically realistic carotid flow rate waveform [7], with a mean flow rate of 6.00 mL/s and a peak flow rate of 23.46 mL/s, was prescribed at the common carotid artery (CCA) inlet of the model.

Reference velocity vectors were generated over a regular grid, by resampling of pre-computed CFD velocity field using 1-mm isotropic volumetric spacing which produced velocity vectors at 20,790 coordinates over a grid of 27mm x 11 mm x 70 mm. The reference velocities were then generated for various phases of the cardiac cycle, including peak systole (for maximum velocities), maximum deceleration in late systole, dichrotic notch (for minimum velocities), diastole (for average velocities), and end diastole.

The accuracy of 1, 2, 3, 4, 5, and 6R was determined in reconstructing time-dependent velocity field [8-11] and compared it with the CFD generated velocity field. Doppler shifts seen by every receiver for a configuration were determined and checked for the wall filter threshold. A linearly least square (LLS) method was applied to calculate the final velocity from the all the receivers with Doppler shifts above the wall filter. Equally weighted LLS method was used to reconstruct the final velocity when the number of receivers with Doppler shifts above the WF was equal to (for 1R to 3R) or less than (for 4R to 6R) the number of receivers for a given configuration. Otherwise, a weighted LLS method was used. To assess the accuracy of each configuration, relative errors in the reconstructed velocity vectors were calculated by comparing the reconstructed velocities with the CFD velocities. For application specific accuracy assessment, maximum shear stress was calculated from the reconstructed velocities and compared with that calculated from CFD velocities by determining the relative error in shear stress values through the vessel.

C. *Experimental Validation*

To experimentally validate the numerical results, a gravity fed parabolic flow was established in a long horizontal cylindrical acrylic tube with an internal diameter (ID) of one inch. Measurements were made after an entrance length of greater than 1 m, where a wall-less agar-based tissue-mimicking material, (TMM) lumen [12] was made as an extension to the long acrylic tube. The outlet of this lumen was then connected to a shorter acrylic tube of same diameter. A blood mimicking fluid (BMF) [13] with a viscosity of 4.0 cP was used. Both TMM and BMF allow the speed of sound to be 1540 m/s to minimize refraction. The height of the inlet reservoir controls the

maximum flow rate, but for lower flow rates, different ID tubing attachments are used. The outlet reservoir collects the fluid for feedback.

For data acquisition, a custom code was written in C++ to run on the Ultrasonix SonixRP. The transmit beam was focused at a required depth but the receive signal was unfocused and acquired simultaneously from all 128 channels using a DAQ system connected to the SonixRP. The data were acquired using a linear array (L14-5/38), transmitting from the center 64 channels, with a transmit frequency of 5 MHz, 1-kHz pulse repetition frequency (PRF), and an ensemble size of 500 pulses. The received signal was post-processed in MATLAB, forming two receivers, using 32 channels each, at either end of the linear array. Each beam was steered at a user-assigned inter-beam angle to focus at a region of interest. These 32 channels from each side were slid towards the center of the array to get data from shallower depth without changing the inter-beam angle. Signal processing was performed on each beam to get the mean Doppler shift. To mimic the 3R, 4R, and 6R configurations, data were acquired by rotating the linear array twice through 60°; receive beams were then chosen depending on the configuration.

III. Results

A. Numerical Evaluation of Single VelocityEstimation

Fig. 2 shows the number receivers above the wall filter as a function of elevation angle (γ) and the inter-beam angle (β) for 3R, 4R, and 6R configurations for the worst case of azimuth angle (φ) for each configuration with a velocity magnitude of 5 cm/s. The worst case of φ is chosen that gives the minimum region of three or more receivers exceeding the wall filter. Considering γ range of 0° to 90°, for an inter-beam angle of 46°, 3R and 4R configurations have 3 or more receivers above the wall filter (WF) for $\gamma < 60°$ and $83° < \gamma < 64°$ respectively. Whereas for 6R, it is the critical angle for which three or more receivers are above the WF for all possible velocity orientations of a 5 cm/s velocity vector (Fig. 2c); this critical angle exists for only the 6R configuration. At lower inter-beam angles, the range of acceptable γ increases for 3R and 4R but lowers for 6R compared to that at 46°. This reduction in the range for 6R is still greater than that for 3R and 4R, for example, by approximately 8° at β = 20°.

B. Numerical Evaluation of Velocities

Fig. 3 shows the relative errors in velocity magnitudes, for velocities estimated using 2, 3, 4, and 6R configurations, compared with the CFD generated velocities in the central plane of 50% eccentric carotid artery (CA) bifurcation model at a phase of minimum flow rate (post-dichrotic notch) in the simulated carotid flow rate waveform applying a wall filter of 50 Hz and inter-beam angle β = 46°. For 2R (Fig. 3a), errors in CCA and ICA are mostly within 5% due to near laminar flow, but higher errors in the ICA and the ECA arm where the flow is more complex. For 3R (Fig. 3b), a major portion of the error is seen in the ICA and ECA arms, ranging from approximately 10% to 30% error in the velocity estimation and is from 24% of the lumen volume. 4R shows improvement in the ICA except distal to the stenosis; error in the CCA and ECA is within the acceptable noise level (less than 5%), which occupies from 72% of the volume. 6R shows improvement in the ICA distal to stenosis thus improving by 4% of the volume compared to 4R, compared to the 4R configuration. 19% or more of the volume along the wall has very low velocities, these velocities are always below the wall filter and are not detected by any number of receiver configuration, therefore show as 100% error in the velocity estimation. The errors calculated in free shear stress relative to the CFD-calculated shear stress, with same parameters used in Fig. 3, show almost similar trend in error distribution as that seen for the velocity error. The improvement in percent volume with error greater than 5% is now 9% for 6R instead of 4% when compared to 4R configuration.

Fig. 4 shows the sensitivity of various multiple receiver configurations to rotation about x, y, and z axes, for the same parameters used in Fig. 3. No sensitivity is observed for rotation about the y-axis for all receiver configurations (not shown). The 3R shows sensitivity to rotations about the x and z axes, whereas 4R is sensitive only to rotation about the z axis at angles of around 18°± 2° (Fig, 4a and 4c). The 6R is insensitive to any rotation.

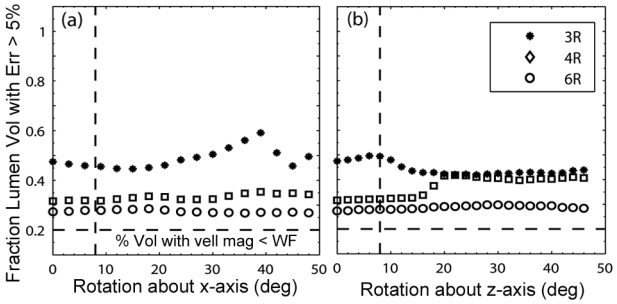

Fig. 4. Orientation sensitivity shown for 3, 4, and 6R configuration by plotting the fraction of the lumen volume contributing to > 5% error in the velocity estimation as function of system rotation about (a) x-axis and (b) z-axis.

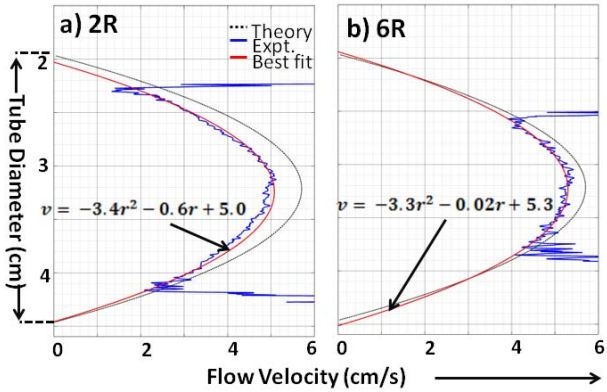

Fig. 5. Estimated velocity magnitude profiles of flow through a straight tube of 1 inch internal diameter for a flow rate of 14 ml/s for (a) 2R, (b) 6R configurations, overlapped with their best fit curves, and theoretical profile is the reference profile.

C. Experimental Vallidation

Fig. 5 shows velocity magnitude profiles estimated using 2R and 6R configurations, along with their best-fit curves and the theoretical flow profile for parabolic flow in a horizontal tube of 1 inch diameter at a constant flow rate of 14 ml/s. The maximum centerline velocity estimated from the best-fit parabolic equations (shown in Fig. 5a & b)) for each configuration is 5.0

cm/s and 5.3 cm/s with standard deviations of 0.19 cm/s and 0.24 cm/s respectively. The percent error relative to theoretically calculated peak velocity of 5.7 cm/s is 12±3% and 7±4% for the 2R and 6R, respectively. The range of velocities for which each configuration has a velocity profile is approximately 1.4 cm/s to 5.0 cm/s for the 2R and 4 cm/s to 5.3 cm/s for the 6R configuration. Outside of this range magnitude of velocities drop to such lower values that there is a greater reduction in the signal-to- noise ratio, making the signal very noisy. This happens for higher parabolic velocities for 6R than 2R because off-axis beams (not in-line with the lumen center axis) for 6R see lower velocity components due to flow being along the lumen

IV. DISCUSSION & CONCLUSION

Numerical results for multi-receive VDUS systems demonstrate that number of receivers is linked with the inter-beam angle, wall filter, system orientation sensitivity, and the complexity of flow. For example, for complex flow in the CA bifurcation, it is shown that increasing the number of receivers improves velocity estimation in more complex flow regions. Increasing this also reduces sensitivity to orientation of the system. It can be suggested from the results that 4 and higher configurations should be the choice for accurate velocity estimations

From initial experimental results, it is shown that 6R gives improved velocity estimates compared to 2R, but this improvement occurs for a smaller central portion of the velocity profile in the lumen compared to 2R. This may in part be due to reduced signal-to-noise ratio introduced by the off-axis beams in the 6R which see only the components of these velocities. 2R being aligned to the flow see actual velocities, therefore encounters this problem for lower velocities. To make any definitive conclusion further investigation at various flow rates including 3R and 4R is needed.

ACKNOWLEDGMENT

The authors would like to acknowledge and thank William Handler, Phin Perquin, John deBryun, and Janet Powell for their assistance. Funding is acknowledged from the Natural Science and Engineering Research Council of Canada, CIHR Training Fellowship in Vascular Research, Canada Foundation for Innovation, and the Ontario Ministry of Research and Innovation.

REFERENCES

[1] L. B. Morgenstern et al, “The risk and benefits of carotid endarterectomy in patients with near occlusion of the carotid artery. North American Symptomatic Carotid Endarterectomy Trial (NASCET) Group,” Neurology, vol. 48, no. 4, 911-5, 1997.

[2] R. Steel and P. J. Fish, “Sample volume misregistration in linear array-based dual beam Doppler ultrasound systems,” IEEE Transaction on Ultrasonics, Ferroelectrics, and Frequency Control, vol. 50, no. 7, pp. 836-47, 2003.

[3] R. F. Smith, B. K. Rutt, A. J. Fox, and R. N. Rankin, “Geometric characterization of stenosed human carotid arteies,” Academy of Radiology, vol. 3, pp. 898-911, 1996.

[4] D. J. Phillips, K. W. Beach, J. Primozich, and D. E. Strandness Jr., “Should the results of ultrasound Doppler studies be reported in units of frequency or velocity?,” Ultrasound in Medicine and Biology, vol. 15, no. 3, pp. 205-12, 1989. Methods in Applied Mechanics and Engineering, vol 178, pp. 39-50, 1999.

[5] P. D. Minev and C. R. Ethier, “A characteristic/finite element algorithm for the 3D Navier-Stokes equations using unstructured grids,” Computer Methods in Applied Mechanics and Engineering, vol 178, pp. 39-50, 1999.

[6] C. R. Ethier, S. Prakash, D. A. Steinman, R. L. Leask, G. G. Couch, and M. Ojha, “Steady flow separation patterns in a 45 degree junction,” Journal of Fluid Mechanics, vol. 411, pp. 1-38, 2000.

[7] D. W. Holdsworth, C. J. D. Norley, R. Frayne, D. A. Steinman, and B. K. Rutt, “Characterization of common carotid artery blood-flow waveforms in normal human subjects,” Physiological Measurement, vol. 20, pp. 219-40, 1999.

[8] M. Calzolai et al, “A 3-D PW Ultrasonic Doppler flowmeter: theory and experimental characterization,” IEEE Transactions on Ultrasonics, Ferroelectrics, and Frequency Control, vol. 46, no. 1, 1999.

[9] B. Dunmire, K. W. Beach, K-H. Labs, M. Plett, and D. E. Strandness Jr., “Cross-beam vector Doppler ultrasound for angle-independent velocity measurements,” Ultrasound in Medicine and Biology, vol. 8, pp. 1213-35, 2000.

[10] D. Vilkomerson, T. Chilipka, R. Outcault, and K. Goldman, “An instrument for screening for carotid stenoses,” Proceedings of the IEEE Ultrasonics Symposium, pp. 393-98, 2005.

[11] S. Uematsu, “Determination of volume of arterial blood flow by an ultrasonic device,” Journal of Clinical Ultrasound, vol. 9, pp. 209-16, 1981.

[12] N.K.. Ramnarine, T. Anderson, and P. R. Hoskins, “Construction and Geometric Stability of Physiological Flow rate wall-less Stenosis Phantoms,” Ultrasound in Medicine and Biology, vol. 27, pp. 245-50, 2001.

[13] N.K.. Ramnarine, D. K. Nassiri, P. R. Hoskins, and J. Lubbers, “Validation of New Blood-Mimicking Fluid for use in Doppler Test Objects,” Ultrasound in Medicine and Biology, vol. 24, pp. 451-59, 1998.